Journal of Advanced Research 20 (2019) 91–104

Contents lists available at ScienceDirect

Journal of Advanced Research

journal homepage: www.elsevier.com/locate/jare

Original Article

Highly biodegradable and bioactive Fe-Pd-bredigite biocomposites prepared by selective laser melting

Chengde Gao [a], Meng Yao [a], Sheng Li [a], Pei Feng [a], Shuping Peng [d,e], Cijun Shuai [a,b,c,*]

[a] State Key Laboratory of High Performance Complex Manufacturing, College of Mechanical and Electrical Engineering, Central South University, Changsha 410083, China
[b] Jiangxi University of Science and Technology, Ganzhou 341000, China
[c] Shenzhen Institute of Information Technology, Shenzhen 518172, China
[d] NHC Key Laboratory of Carcinogenesis and The Key Laboratory of Carcinogenesis and Cancer Invasion of the Chinese Ministry of Education, Xiangya Hospital, Central South University, Changsha 410013, China
[e] Cancer Research Institute, School of Basic Medical Sciences, Central South University, Changsha 410013, China

HIGHLIGHTS

- A Fe-based biocomposite containing Pd-rich phases and bredigite was developed.
- The degradation rate was significantly elevated due to the microgalvanic corrosion.
- The degradation of bredigite provided more channels for corrosion penetration.
- The biocomposites featured comparable strength and hardness with the native bone.
- The biocomposites showed excellent bioactivity and favorable biocompatibility.

GRAPHICAL ABSTRACT

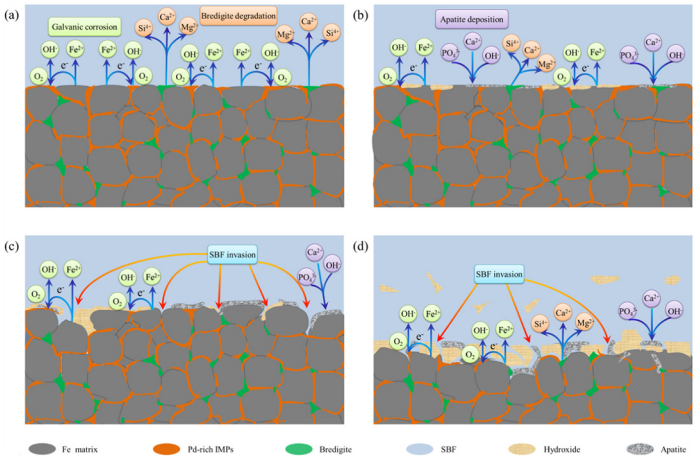

Schematic illustration of the rapid degradation and apatite deposition process for Fe-Pd-bredigite biocomposites.

ARTICLE INFO

Article history:
Received 25 April 2019
Revised 6 June 2019
Accepted 17 June 2019
Available online 19 June 2019

Keywords:
Iron-based biocomposites
Palladium
Bredigite
Biodegradability

ABSTRACT

Iron (Fe) has been highly anticipated as a bone implant material owing to the biodegradability and excellent mechanical properties, but limited by the slow degradation and poor bioactivity. In this study, novel Fe-palladium (Pd)-bredigite biocomposites were developed by selective laser melting aiming to improve both the degradation behavior and bioactivity of Fe. The results showed that most Pd formed Pd-rich intermetallic phases (IMPs) with a nearly continuous network while the bredigite phase was distributed at the grain boundaries. In addition, a large amount of much nobler IMPs formed micro-galvanic pairs with the Fe matrix, inducing tremendous micro-galvanic corrosion. The IMPs contained a high amount of Pd^{2+} with a high reduction potential, which further promoted the efficiency of micro-galvanic corrosion. Moreover, the rapid degradation of bredigite also facilitated the penetration of the corrosion medium. As a result, the Fe-4Pd-5bredigite biocomposite showed a uniform degradation with a rate that is 6

Peer review under responsibility of Cairo University.
* Corresponding author.
E-mail address: shuai@csu.edu.cn (C. Shuai).

https://doi.org/10.1016/j.jare.2019.06.001

Bioactivity
Selective laser melting

times that of Fe. Furthermore, the developed Fe-Pd-bredigite biocomposites also featured excellent bioactivity, cytocompatibility, and suitable mechanical properties as characterized by the rapid apatite deposition, normal proliferation of human osteoblast-like cells (MG-63), and comparable strength and microhardness with the native bone. Overall, this study opens a new avenue for improving both the degradation and bioactivity of Fe-based composites and may facilitate their applications as biodegradable implants for tissue/organ repair.

Introduction

Biodegradable metals have received increasing attention as temporary bone implant materials over the past years [1]. Among these metals, iron (Fe) possesses the most attractive mechanical properties for load-bearing applications. Fe is also an important biogenic element in the human body and participates in many physiological functions, such as oxygen transport, electron transfer and catalysis [2]. Additionally, Fe has good biocompatibility with very limited or no toxicity to cells, tissues and organs, which has been demonstrated in many *in-vitro* and *in-vivo* studies [3,4]. Therefore, Fe has been considered as a promising candidate for use as biodegradable implants. However, so far, the applications of Fe-based bone implants are limited due to the very slow degradation in physiological media and poor interfacial bonding with the native bone [5].

It is known that an ideal bone implant should not only progressively degrade at a suitable rate (approximately 0.2–0.5 mm·year^{-1}) to match the bone healing process, but also be bioactive (capability of direct bonding to the native bone) to facilitate the bone healing process [6–10]. To accelerate degradation, current studies on Fe-based implants have been mainly focused on alloying, surface coating, patterning, surface treatment, new fabrication methods and texturing. Cheng et al. deposited micro-patterned gold (Au) disc arrays [11], whereas Huang and Zheng deposited platinum (Pt) disc arrays [12] on the surface of pure Fe, respectively. The results indicated accelerated biodegradation due to the galvanic corrosion between the micro-patterned discs and Fe matrix. A similar coating method was also reported in poly(lactide-co-glycolide)-coated magnesium (Mg) alloys [13]. Zhou et al. reported significantly higher degradation rate of biodegradable Fe implants after surface treatment with sandblasting, which was attributed to the special properties of sandblasted surfaces, including surface composition, high roughness and high density of dislocations [14]. Bagherifard et al. treated the surface of a Mg alloy by severe shot peening and revealed that a slight grinding after shot peening led to an the improvement in electrochemical corrosion characteristics [15]. In addition, magnetron sputtering in combination with ultra violet ray lithography was also tried in fabricating Fe foils for use as biodegradable implants [16]. The Fe foils exhibited a preferential orientation in the ⟨1 1 0⟩ direction and -fine grain structure, as well as corrosion rates of approximately 0.1 mm·year^{-1}. An electroforming technique was developed for fabricating biodegradable Fe foils [17], and the results showed that the electroformed Fe possessed a fine-grain microstructure and faster degradation than those of Fe fabricated by casting and thermomechanical treatment. The effects of the rolling mode on the micro-texture evolution and biodegradation behavior of polycrystalline Fe as a biodegradable implant material were investigated by Obayi et al. [18]. The results indicated that cross-rolled samples recrystallized with lower rates than the straight-rolled ones, and no relevant differences in the corrosion rate were observed between them, except for a more uniform degradation for cross-rolled samples.

As for alloying, the selection of alloying elements basically considers two criteria [9,19]: (I) less noble alloying elements to increase the corrosion susceptibility of the Fe matrix, and (II) nobler alloying elements and/or formation of intermetallic phases (IMPs) to induce galvanic corrosion with the Fe matrix. So far, manganese (Mn), silicon (Si), tin (Sn), and carbon (C), etc., have been alloyed into Fe and enhanced both the degradation rate and mechanical properties of the matrix [20–23].

As a noble metal, palladium (Pd) has a higher standard potential than Fe and is likely to form IMPs containing high amounts (at least 50 at.%) of Pd^{2+} due to the limited solubility in Fe. More importantly, the standard reaction potential of $Pd^{2+} + 2e^- \rightarrow$ Pd (E = 0.915 V [24]) is higher than that of most alloying elements. These two characteristics make the resulting Pd-rich IMPs much nobler than other IMPs, when compared with the Fe matrix. Thus, the introduction of Pd is expected to induce tremendous micro-galvanic corrosion, thereby increasing the degradation rate of Fe. In addition, Pd has been commonly used in orthodontic and anti-neoplastic applications and is considered to be tolerable by the body [25–27]. Nevertheless, Pd may induce cytotoxicity at high concentrations and biocompatibility is still a crucial concern for bone repairs.

To improve both the biocompatibility and bioactivity of Fe-Pd alloy, metal matrix composites (MMCs) with bioceramics may be a feasible approach because the performance of MMCs can be modified by varying the composition and distribution of the ceramic phase [28]. Compared with the commonly used calcium (Ca)-phosphorus (P) bioceramics, bredigite ($Ca_7MgSi_4O_{16}$) has been recently evaluated as a promising bioceramic with a combination of outstanding bioactivity, excellent biocompatibility, and high mechanical strength [29]. Bredigite can rapidly induce apatite mineralization and form a strong chemical bonding with bone tissues. Moreover, the main components of bredigite, i.e., Ca, Mg and Si, can also facilitate the growth of cells and bone tissues [30]. These discoveries have stimulated the exploration of Fe-Pd-bredigite biocomposites with accelerated biodegradation, excellent bioactivity and favorable biocompatibility.

So far, Fe-based biocomposites have been fabricated by spark plasma sintering (SPS), powder metallurgy, pulsed electric current assisted sintering, etc. For example, Zheng et al. fabricated Fe-Pd and Fe-Pt biocomposites by SPS with powders, which showed a much smaller grain size of SPS composites than that of as-cast Fe [27]. Sikora-Jasinska et al. fabricated Fe/Mg silicide biocomposites using different powder metallurgy techniques and found that the preparation method of the composite powder played a major role in the corrosion process and mechanism of the final biocomposites [31]. Montufar et al. developed alpha tricalcium phosphate (α-TCP)/Fe biocomposites consolidated by pulsed electric current-assisted sintering to minimize the processing time and temperature while improving their performance [32]. As one of the additive manufacturing techniques, selective laser melting (SLM) is capable of manufacturing parts directly from three-dimensional (3D) models without the need of supporting structures or molds [33,34]. This technique enables the rapid

manufacturing of custom-designed implants with complex shapes and internal structures, particularly suitable for biomedical applications [35]. Moreover, SLM can easily obtain a fine microstructure of alloys via rapid melting/solidification [36,37]. The out-of-equilibrium process is also able to extend the solid solution limits of alloying elements and decreases composition segregation, thereby resulting in homogeneous textures [38].

This study aims to develop an Fe-based biocomposite containing homogenously dispersed Pd-rich IMPs and bredigite phase in order to (i) accelerate Fe degradation and (ii) improve the bioactivity and biocompatibility simultaneously. The Fe-Pd-bredigite biocomposites were fabricated by SLM. The effects of chemical composition on the microstructure, biodegradability and bioactivity of the biocomposites were systematically investigated. Particular attention was paid to exploring the potential mechanisms for the improved biodegradation and bioactivity. Additionally, the mechanical performance and *in vitro* cell behavior were also investigated in detail.

Experimental

Materials and sample preparation

Fe powder (purity 99.9%, Shanghai Naiou Nano technology Co., Ltd., Shanghai, China), bredigite powder (purity 99.9%, Kunshan Huaqiao Science and Technology New Material Co., Ltd., Suzhou, China), and Pd powder (purity 99.9%, Beijing Deke Island Gold Technology Co., Ltd., Beijing, China) were used as raw materials. A series of mixed powders were obtained by mixing the three powders using a ball mill (DECO-PBM-V-0.4L, Changsha Deco Equipment Co., Ltd., Changsha, China) at a rotational speed of 260 rpm for 4 h. The morphology and composition of the powders were analyzed by using a scanning electron microscope equipped with an energy dispersive spectroscope (SEM/EDS, Phenom Prox, Phenom-World BV, Eindhoven, Netherlands). The particle size distribution was measured by a laser diffraction particle size analyzer (Mastersizer 3000, Malvern Instruments Ltd., Malvern, UK) with a Hydro EV dispersion unit. The mixed powders were then used for sample preparation on a custom-made SLM system with a laser power of 90 W, a scanning speed of 20 $mm{\cdot}s^{-1}$, a hatch distance of 0.08 mm and a layer thickness of 0.1 mm. The laser scan followed an oscillation deposition strategy with a rotation of $\sim 67^{\circ}$ between successive layers to relieve stresses. It should be noted that the weight ratio of Pd in this study was set as 2 and 4 wt%, respectively, as a higher amount of Pd may induce severe cytotoxicity [39]. The detailed composition of the prepared Fe-Pd-bredigite biocomposites is presented in Table 1.

Microstructural characterization

For metallographic analysis, the samples were mounted in epoxy and mechanically ground successively with 800, 1000 and 1600 grit sandpapers, and then polished with diamond pastes, followed by ultrasonic cleaning and air-drying. Subsequently, the metallographic structure of Fe-Pd-bredigite biocomposites was observed using an optical microscope (PMG3, Olympus, Tokyo, Japan) and the grain sizes were determined by the linear intercept method using the ImageJ software. In addition, the phase composition of the Fe-Pd-bredigite biocomposites was analyzed by X-ray diffraction (XRD, D8 Advance, Bruker AXS, Karlsruhe, Germany) with Cu-Kα radiation. The scanning rate, accelerating voltage and current were set as $8^{\circ}{\cdot}min^{-1}$, 40 kV and 100 mA, respectively. To determine the distribution states of Pd and bredigite in the Fe matrix, the microstructure and elemental composition of the Fe-Pd-bredigite biocomposites were examined by the SEM/EDS.

Table 1
The composition of iron (Fe)-palladium (Pd)-bredigite biocomposites.

Formulation	Composition (wt.%)		
	Fe	Pd	Bredigite
Fe-2Pd-2.5bredigite	95.5	2	2.5
Fe-2Pd-5bredigite	93	2	5
Fe-2Pd-10bredigite	88	2	10
Fe-4Pd-2.5bredigite	93.5	4	2.5
Fe-4Pd-5bredigite	91	4	5
Fe-4Pd-10bredigite	86	4	10

Mechanical tests

The compressive properties of the Fe-Pd-bredigite biocomposites were evaluated by compression tests, which were carried out on a universal testing machine (WDW-100M, Jinan Zhong Lu Chang Test Machine Manufacturing Co., Ltd., Jinan, China) with a crosshead speed of 5×10^{-4} $m{\cdot}min^{-1}$. The test samples were cylindrical with dimensions of 5 mm in height and 2 mm in diameter. In addition, the microhardness of the Fe-Pd-bredigite biocomposites was measured by a microhardness tester (HXD-1000TM/LCD, Shanghai Taiming Optical Instrument Co., Ltd., Shanghai, China) with a load of 2.94 N and a dwell time of 15 s. The morphology of the indentations was also observed using the SEM. At least five measurements were repeated for each group in all the mechanical tests.

Biodegradation tests

Electrochemical tests and immersion tests were both carried out in a simulated body fluid (SBF) solution at 37 °C. The SBF solution consisted of (in $g{\cdot}L^{-1}$): 0.3050 $MgCl_2{\cdot}6H_2O$, 6.5453 NaCl, 0.2681 $Na_2HPO_4{\cdot}7H_2O$, 0.3676 $CaCl_2{\cdot}2H_2O$, 0.3728 KCl, 2.2683 $NaHCO_3$, 6.0570 $(CH_2OH)_3CNH_2$, and 0.0711 $NaSO_4$ according to the literature [40]. In addition, the pH of the SBF solution was adjusted to 7.4 by using hydrochloric acid (1 $mol{\cdot}L^{-1}$). The electrochemical properties of the Fe-Pd-bredigite biocomposites were examined using an electrochemical workstation (CHI604D, CH Instruments Inc., Shanghai, China). Prior to the tests, the samples were mounted in epoxy with a surface exposure of 1 cm^2, followed by grinding, polishing, cleaning and drying. During the electrochemical tests, the mounted samples acted as the working electrode while a saturated calomel electrode and a platinum electrode acted as the reference electrode and counter electrode, respectively. The open circuit potentials were stabilized by immersing the samples in the SBF solution. Afterwards, the potentiodynamic polarization curves were recorded at a scanning rate of 0.5 $mV{\cdot}s^{-1}$. The corrosion potentials (E_{corr}), corrosion current densities (I_{corr}) and degradation rates were then acquired obtained using the Tafel extrapolation method.

Immersion tests were performed in the SBF at 37 °C for 21 d. During immersion, the SBF solution was regularly replaced by a fresh one every 3 d to simulate the *in-vivo* corrosion environment. After immersion, the samples were ultrasonicated in ethanol and then dried at room temperature. The corrosion morphology and elemental composition after immersion were characterized by the SEM/EDS. Afterwards, the samples were vigorously stirred in a solution containing 100 mL hydrochloric acid, 5 g stannous chloride, and 2 g antimonous oxide to remove the corrosion products, followed by rinsing with deionized water and ethanol and blow-drying. The 3D surface profiles of the samples were then analyzed by a Veeco Wyko NT9100 optical profile tester (Veeco Instruments Inc., Plainview, USA).

Cell culture tests

In vitro cell culture tests were performed using an indirect contact method because the indirect method enables not only an extensive contact of the materials with cells but also an analysis of the toxic effects of various components and concentrations on cells. Human osteoblast-like cells (MG-63, American Type Culture Collection, Manassas, USA) were used to assess the *in vitro* cytocompatibility of the Fe-Pd-bredigite biocomposites. The MG-63 cells were pre-cultured in Dulbecco's modified eagle medium (DMEM), which contained 100 $U \cdot mL^{-1}$ penicillin, 100 $mg \cdot mL^{-1}$ streptomycin, and 10% fetal bovine serum. At the same time, the samples were immersed in a separate DMEM with a sample surface area to extract a volume ratio of 1.25 $cm^2 \cdot mL^{-1}$ for 3 d, which was determined to be consistent with that of the immersion tests for correlating the results of the two tests. The resulting extracts were collected for subsequent tests.

To evaluate the cell morphology, the MG-63 cells were incubated in DMEM at 37 °C in 24-well plates. After 4 h, the cultured medium of each well was replaced by the aforementioned extracts of the Fe-Pd-bredigite biocomposites. Meanwhile, a complete medium without extracts served as the control group. The cells were further cultured for 5 d, gently rinsed using a phosphate buffered solution, and then stained by Ethidium homodimer-1 and Calcein-AM reagents for 20 min. Afterwards, the cells were fixed with glass slides and a fluorescence microscope (BX60, Olympus, Tokyo, Japan) was employed to observe the cell morphology.

For cell viability tests, the MG-63 cells were cultured for 24 h in 96-well plates with a seeding density of approximately 2×10^3 cells per 100 μL DMEM, which was then replaced by the extracts.

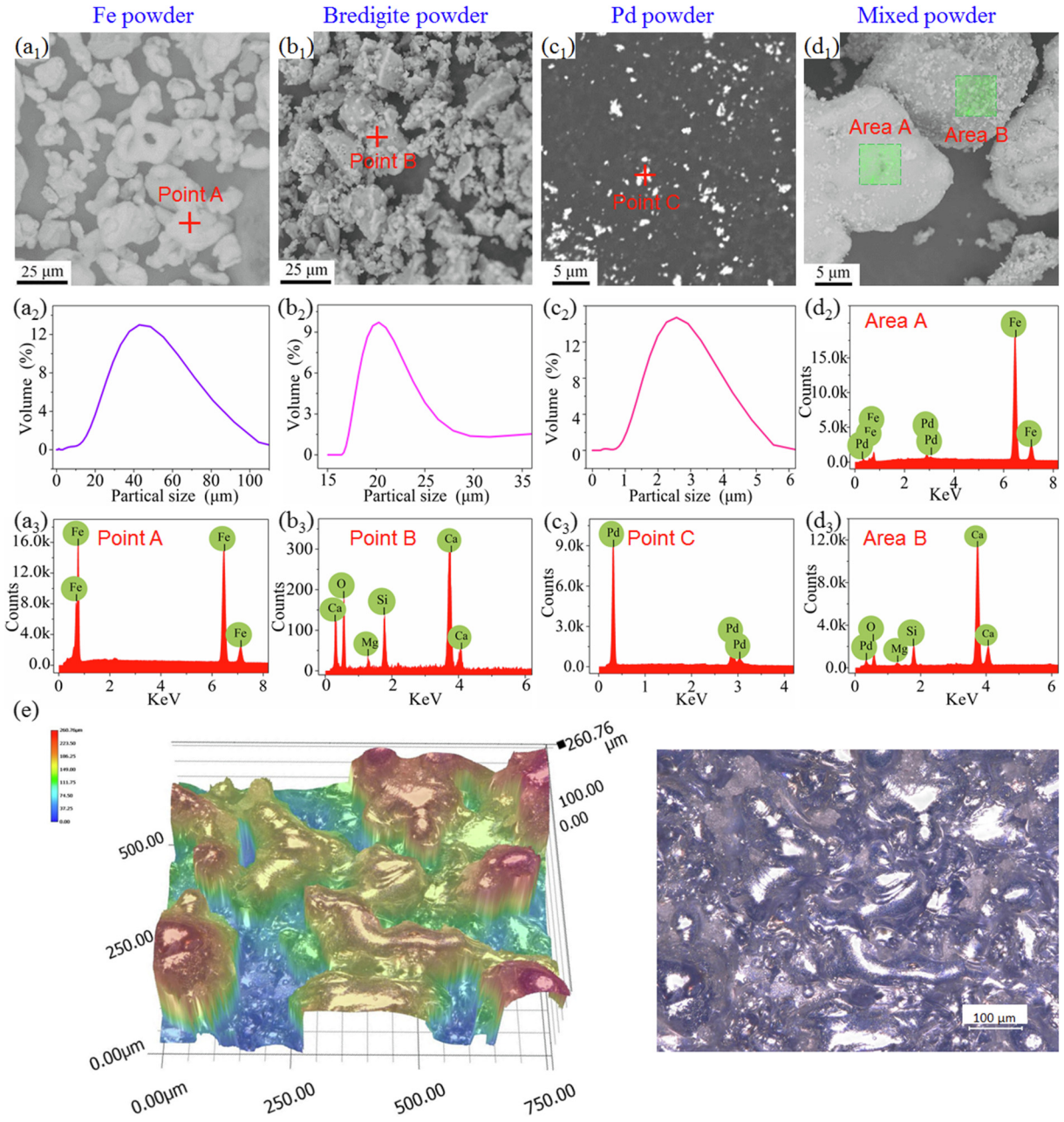

Fig. 1. (a_1–d_1) Scanning electron microscope (SEM) morphology, (a_2–c_2) particle size distribution and (d_2, a_3–d_3) element composition of the iron (Fe), palladium (Pd), bredigite and mixed powders. (e) Typical surface profile of the original Fe-Pd-bredigite biocomposites prepared by SLM.

DMEM without extracts served as the control group. After 3 and 5 d of culture, a cell counting kit-8 (CCK-8) solution with a volume of 10 μL was dropped into each well and the cells were continually cultured for 2 h. Subsequently, the absorbance was determined using Paradigm™ Detection Platform (Beckman Coulter, Fullerton, USA) at a wavelength of 450 nm, and the cell viability (V) was calculated according to Equation (1):

$$V = OD_i/OD_0 \quad (1)$$

where OD_i $OD_i$is the mean absorbance of the experimental group and $OD_0$$OD_0$ is the mean absorbance of the control group.

Statistical analysis

All experimental data were presented as mean values ± standard deviations and statistically analyzed by ANOVA. The differences were considered significant when $P < 0.05$.

Results

Powder characterization and SLM preparation

The morphology, composition and size distribution of the powders used in this study are shown in Fig. 1. It can be observed that

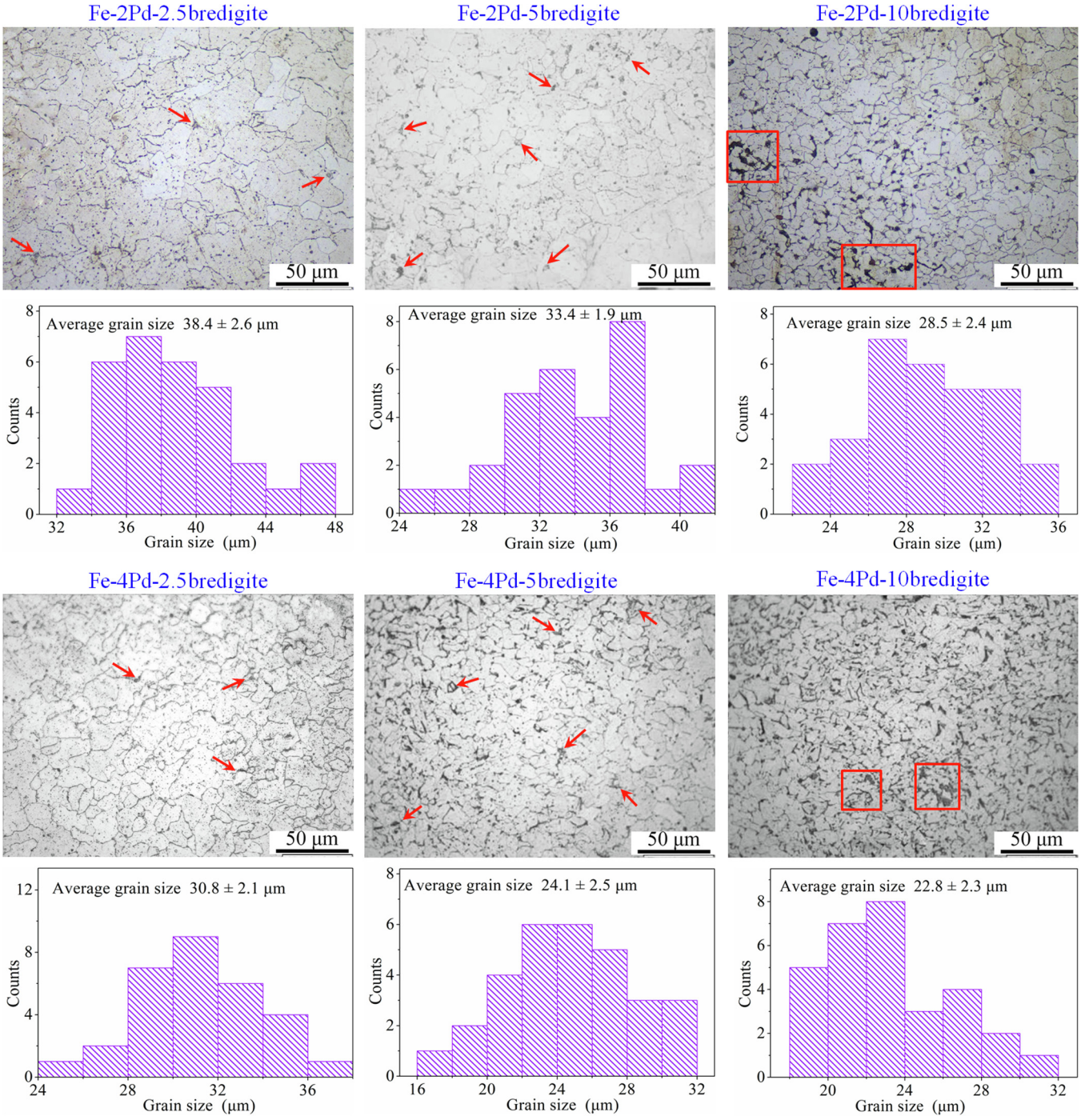

Fig. 2. Metallographs and corresponding grain size distribution of the prepared Fe-Pd-bredigite biocomposites.

the Fe powder consisted of light-gray particles in near-spherical shape and the quantitative result showed a particle size range of approximately 20–100 μm (Fig. 1a1 and a2). The EDS spectrum at point A presented strong peaks corresponding to only Fe (Fig. 1a3), indicating a high purity of the powder. In comparison, the dark-gray bredigite powder showed a mixture of large polygonal particles in tens of micrometers and small irregular particles in several micrometers (Fig. 1b1). The size distribution result indicated that most of the bredigite particles were in the size range of 17–30 μm (Fig. 1b2). The EDS analysis at point B presented the typical peaks of Ca, Si, Mg and O (Fig. 1b3), corresponding to the stoichiometric ratio of bredigite. As observed from Fig. 1c1 and 1c2, the Pd particles presented a spherical morphology in bright colors and the particle size was distributed in the range of 1–6 μm. The EDS spectrum at point C indicated strong peaks of Pd with no other elements (Fig. 1c3). The morphology of the ball-milled mixed powder is shown in Fig. 1d1, in which bredigite particles were observable among Fe particles and Pd was homogenously distributed on both of Fe and bredigite particles. This was further confirmed by the EDS spectra at areas A and B (Fig. 1d2 and 1d3). A surface profile of the original Fe-Pd-bredigite biocomposites is shown in Fig. 1e, which presents a typical rough surface by SLM technology due to balling or partially melted powder [41,42].

Microstructure and phase compositions of the SLM composites

The metallographs and corresponding grain size distribution of the prepared Fe-Pd-bredigite biocomposites are shown in Fig. 2. It can be observed that all the biocomposites possess a regular microstructure mainly consisting of equiaxed grains. The grain size of the biocomposites gradually decreased with the increase in Pd and bredigite. Specifically, there was a 20–28% decrease in grain size between the Fe-2Pd-*x*bredigite and the Fe-4Pd-*x*bredigite biocomposites, but no significant difference in the uniformity of grain size distribution can be observed. For the Fe-*x*Pd-2.5bredigite biocomposites, the grain size distribution was relatively uniform with average values of 38.4 ± 2.6 μm and 30.8 ± 2.1 μm, respectively. In

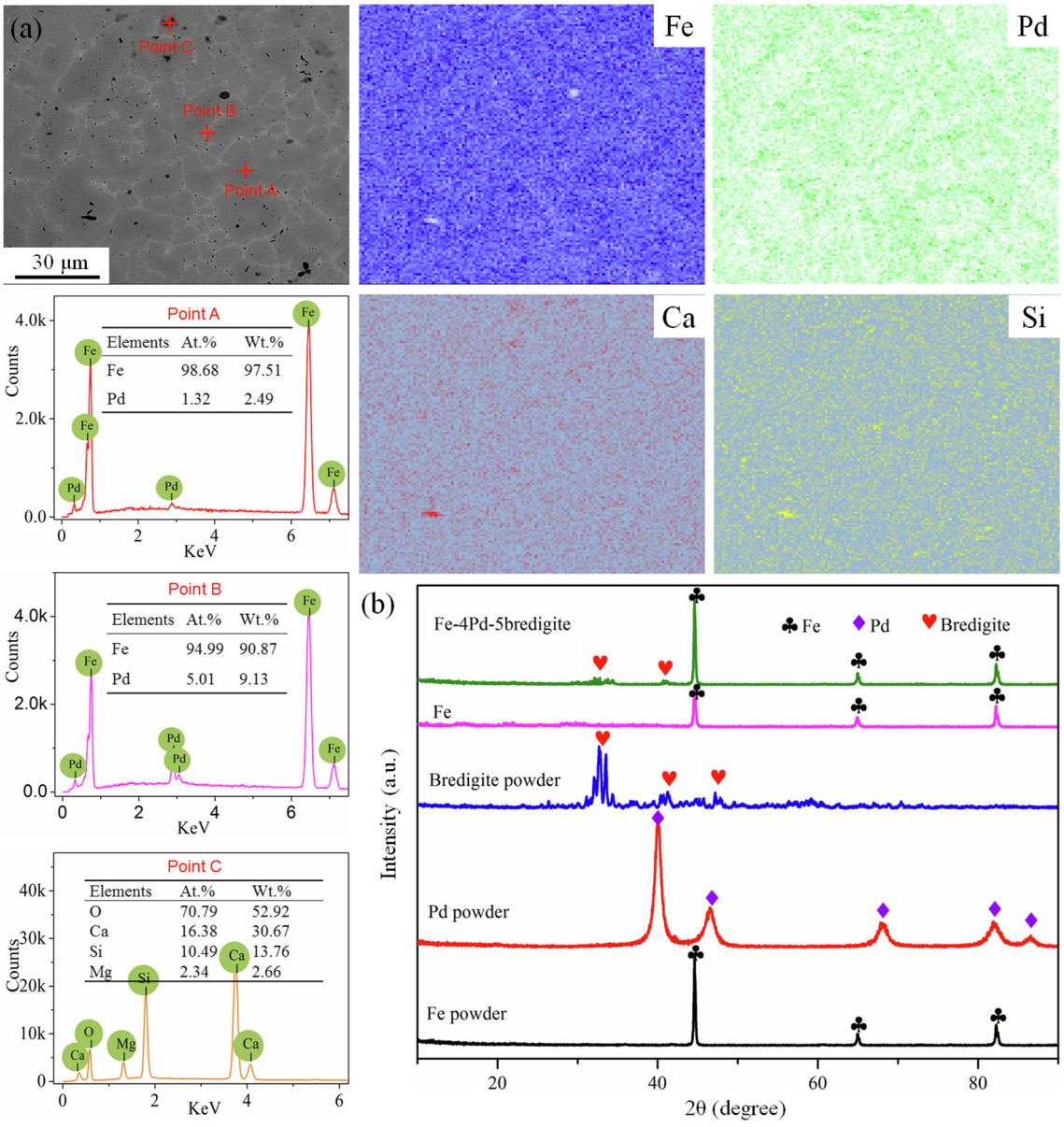

Fig. 3. (a) Surface morphology and corresponding element composition of Fe-4Pd-5bredigite biocomposite; (b) X-ray diffraction (XRD) patterns of Fe and Fe-4Pd-5bredigite biocomposite after laser melting, as well as the raw powders.

comparison, the average grain sizes of the Fe-*x*Pd-5bredigite biocomposites were approximately 33.4 ± 1.9 μm and 24.1 ± 2.5 μm, respectively, which were smaller than those of the Fe-*x*Pd-2.5bredigite biocomposites. Bredigite (indicated by red arrows) was found homogeneously distributed along the grain boundaries in both the Fe-*x*Pd-2.5bredigite and Fe-*x*Pd-5bredigite biocomposites. Nevertheless, many conglomerations appeared at the grain boundaries of the Fe-*x*Pd-10bredigite biocomposites, as indicated by the red rectangles. Moreover, grains with a large variety of sizes and shapes were also observed, especially around those conglomerations. The different grain sizes among the Fe-Pd-bredigite biocomposites could be attributed to the different contents of solid phases, which were believed to inhibit grain growth by promoted supercooling and heterogeneous nucleation.

To reveal the microstructure and compositions of the biocomposites, the typical features of the Fe-4Pd-5bredigite biocomposite were examined using the SEM/EDS. The backscattered electron SEM image in Fig. 3a shows a homogeneous and relatively dense microstructure with different brightness. It was evident that the gray areas corresponded to the Fe matrix. A bright contrast was observed along the grain boundaries, suggesting the enrichment of an element with high atomic weight. Moreover, the enrichment was distributed throughout the grain boundaries, leading to the formation of a nearly continuous network. In addition, some dark areas were also observed within the matrix. EDS image analysis inside the grains (Point A) showed strong peaks of Fe and Pd with a Pd content of 2.49 wt%, which was close to the solubility limit of Pd in Fe. The spectrum of the bright contrast at Point B also showed the peaks of Fe and Pd, except for an elevated Pd content of 9.13 wt %. This implied that Pd was segregated into Pd-rich precipitates at the grain boundaries. The spectrum at Point C (the dark areas) consisted of O, Ca, Si and Mg with atom ratios close to the nominal composition of bredigite. EDS mapping was also performed to obtain a general overview of element distribution, and the results confirmed the enrichment of Pd along the grain boundaries. XRD analysis was conducted to determine the phase composition of the Fe-4Pd-5bredigite biocomposite with Fe and the raw powders as the control (Fig. 3b). As can be observed in the spectra, the raw powders showed typical peaks for Fe (JCPDS card no. 06-0696), Pd (JCPDS card no. 46-1043) and bredigite (JCPDS 36-0399), respectively. After laser melting, the XRD pattern of Fe was similar to that of the Fe powder without detectable peak shifts or phase changes. For the Fe-4Pd-5bredigite biocomposite, Fe was detected as the major phase with small amount of bredigite, but no Pd-rich IMPs were detected because of the limitation of the XRD technique. According to the SEM/EDS and XRD results, the biocomposite presented the coexistence of Fe and bredigite phases, and Pd existed as both solid solution inside the Fe grains and Pd-rich IMPs along the grain boundaries.

Electrochemical behavior and in vitro degradation

To separate the effect of surface roughness from that of the chemical composition, a surface grinding and polishing process was performed before the electrochemical and degradation tests. The electrochemical behavior of the biocomposites was evaluated in the SBF using a short-term polarization measurement and the corresponding potentiodynamic polarization curves are plotted in Fig. 4a. With increasing Pd and bredigite contents, the anodic Tafel slopes became sharper and the polarization curves shifted toward

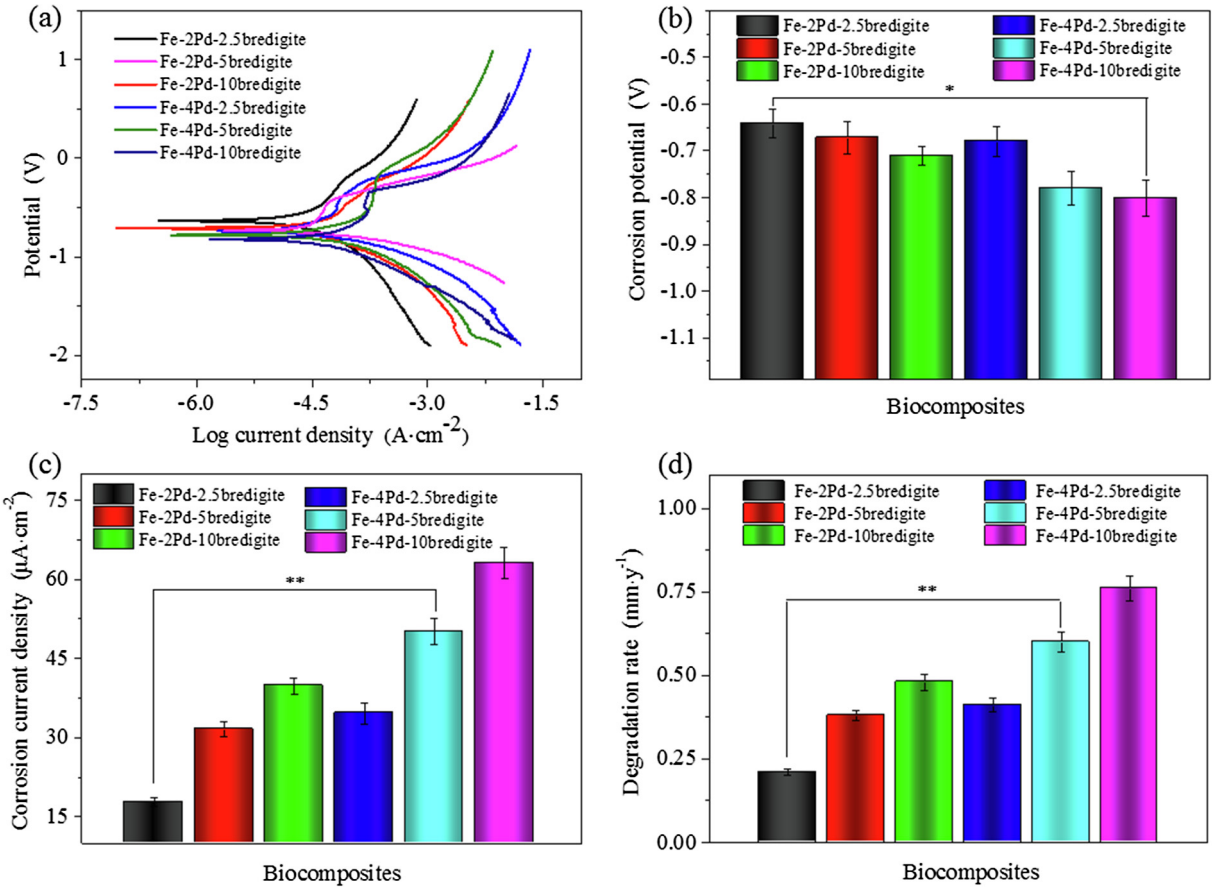

Fig. 4. (a) Potentiodynamic polarization curves, (b) corresponding corrosion potentials (E_{corr}), (c) corrosion current densities (I_{corr}) and (d) degradation rates of Fe-Pd-bredigite biocomposites by electrochemical tests ($^{*}P < 0.05$; $^{**}P < 0.01$).

higher current densities, indicating the faster dissolution of the Fe matrix. Moreover, the polarization curves showed obvious current plateaus, which revealed a passivation behavior during corrosion. Similar phenomenon has been reported in Zinc (Zn)-hydroxyapatite (HAP) composites [43]. The E_{corr}, I_{corr} and degradation rates of the biocomposites were determined by the Tafel extrapolation method and are displayed in Fig. 4b–d. It can be observed that the Fe-4Pd-*x*bredigite biocomposites slightly shifted by approximately −0.038, −0.108 and −0.091 V, respectively, as compared with the Fe-2Pd-*x*bredigite biocomposites. This may be associated with the solubility limit (up to 2 wt% [19]) of Pd in Fe according to the phase diagram. In this case, the residual Pd in the Fe-4Pd-*x*bredigite biocomposites would precipitate into Pd-rich IMPs and form micro-galvanic cells with the matrix. This led to the shifting of the I_{corr} toward much higher values, i.e., from 17.78, 31.62 and 39.81 $\mu A \cdot cm^{-2}$ for Fe-2Pd-*x*bredigite biocomposites to 34.67, 50.12 and 63.09 $\mu A \cdot cm^{-2}$ for the Fe-4Pd-*x*bredigite biocomposites, thereby accelerating the corrosion process. For the Fe-4Pd-*x*bredigite biocomposites, the degradation rates were 0.41, 0.6 and 0.76 $mm \cdot y^{-1}$, respectively, which were higher than those of the Fe-2Pd-*x*bredigite biocomposites. In addition, the biocomposites containing more bredigite generally featured higher degradation rates. This behavior was especially noticeable for Fe-*x*Pd-10bredigite biocomposites, which was about twice that of the Fe-*x*Pd-2.5bredigite biocomposites. Compared with bredigite, Pd showed a better improvement in the degradation rate of Fe. The most remarkable improvements were attained in Fe-4Pd-5bredigite and the Fe-4Pd-10bredigite biocomposites, which both contained high amounts of Pd-rich IMPs and bredigite phase.

Static immersion tests were conducted to investigate the long-term degradation behavior of the biocomposites. The degradation morphology and element composition after 21 d of immersion were analyzed using the SEM/EDS, as shown in Fig. 5. It was worth noting that the grain boundaries were generally the preferred attacked sites of corrosion due to the existence of both Pd-rich IMPs and bredigite. The surface of the Fe-2Pd-2.5bredigite biocomposite was partially covered with a compact and smooth product layer in dark-gray color. The EDS spectrum at Point A revealed Fe and O as the main elements of the corrosion products. Additionally, a few worm-like sediments (indicated at Point B) together with fine and spherical crystallites (indicated at Point C) were also observed at the grain boundaries. Corresponding element analysis showed the co-existence of significant amounts of Ca, Mg and O along with small amounts of Pd, P, Si, Na and C. Because P, Na and C were only present in the SBF solution, the crystallites can thus be identified as apatites while Pd and Si originated from the

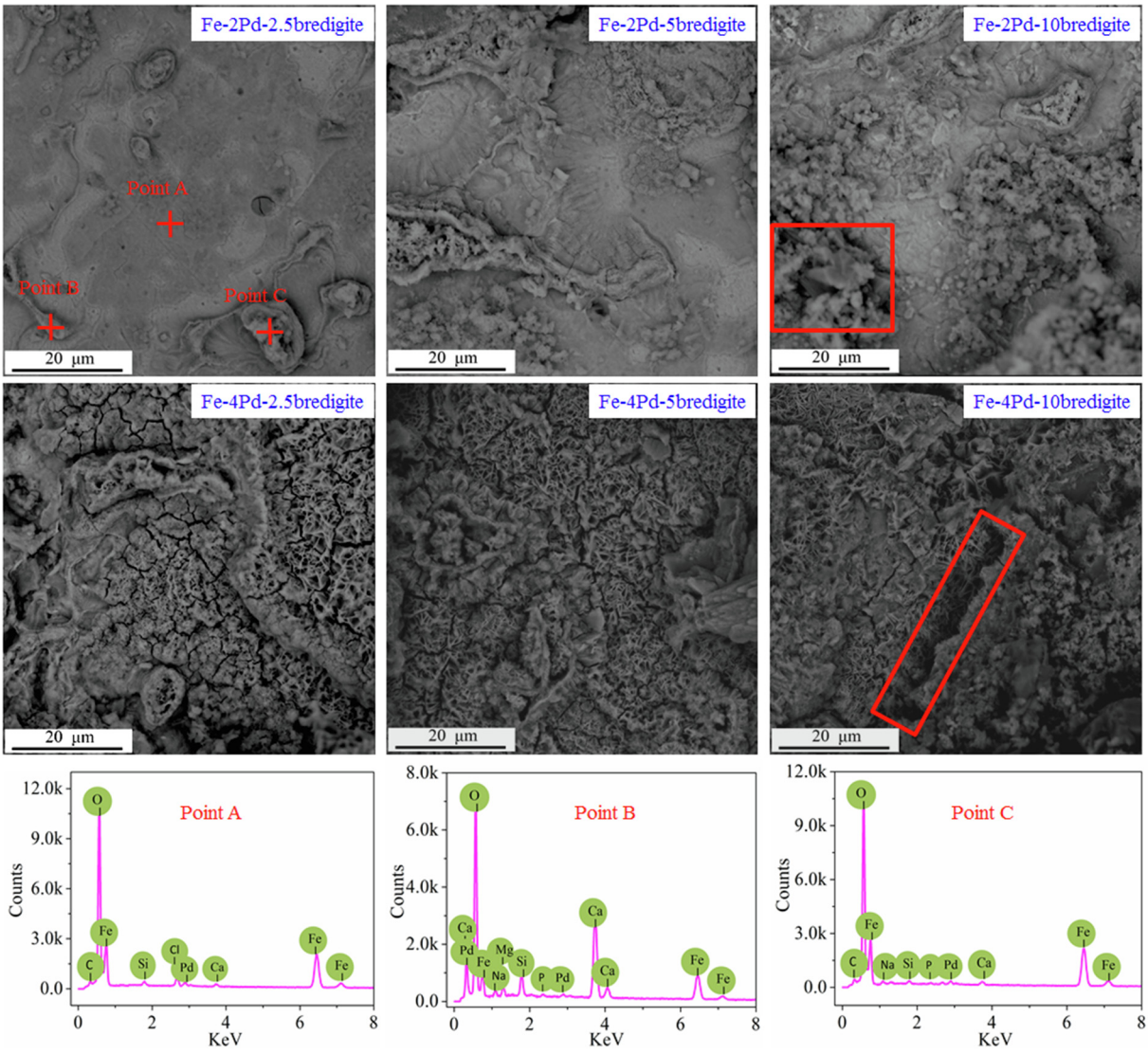

Fig. 5. Degradation morphology and corresponding element composition in the corrosion products of Fe-Pd-bredigite biocomposites after immersion tests for 21 d.

degradation of the biocomposite. In contrast, the Fe-4Pd-2.5bredigite biocomposite were fully covered by broccoli-like products, which were composed of a mixture of Fe oxides and apatites and no clear boundaries were distinguishable between the Fe oxides and apatites. This revealed a strong corrosion attack caused by the galvanic corrosion between Pd-rich IMPs and the Fe matrix. Moreover, the product layer appeared to be loose and porous, which enabled the easy penetration of the corrosion medium into the underneath fresh matrix, thereby accelerating the corrosion process. With increased bredigite content, the corrosion morphology was characterized by more apatite precipitation as well as slight changes in the amount of corrosion products owing to the invasion of the corrosion medium *via* the Fe-bredigite interfaces. The enhanced apatite precipitation was mainly attributed to the excellent bioactivity of bredigite, which could encourage the precipitation of Ca- and P-containing phases. In the presence of corrosion products, the Fe-*x*Pd-2.5bredigite and Fe-*x*Pd-5bredigite biocomposites almost maintained a uniform corrosion mode while localized corrosion with corrosion cavities (as indicated by red rectangles) was observed in the Fe-*x*Pd-10bredigite biocomposites, which might be due to the bredigite conglomerations at the grain boundaries.

To clarify the spatial corrosion process, the 3D surface profile of the biocomposites after product removal is shown in Fig. 6. The color legends displayed on the top left corner of the insets represent the height from the highest points with red to the lowest points with blue. As indicated, the height difference varies with the contents of Pd and bredigite, corresponding to different corrosion features. The Fe-4Pd-2.5bredigite biocomposite showed much severe corrosion compared with the Fe-2Pd-2.5bredigite biocomposite (height difference of 103.01 μm *vs.* 64.81 μm). This phenomenon was also present in Fe-*x*Pd-5bredigite and the Fe-*x*Pd-10bredigite biocomposites. The intensified corrosion at higher Pd content can be attributed to the large volume fraction of Pd-rich IMPs formed at the grain boundaries, which promoted micro-galvanic corrosion and increased the dissolution of Fe. Additionally, the presence of excessive interfaces in the Fe-4Pd-*x*bredigite biocomposites was also responsible for the intensified corrosion by providing more opportunities for the permeation and diffusion of the corrosion medium. In comparison, the height difference first decreased with increasing bredigite from 2.5 wt% to 5 wt% and then increased with increasing bredigite from 5 wt% to 10 wt%, demonstrating a corrosion mode transition from uneven corrosion for Fe-*x*Pd-2.5bredigite to uniform corrosion for Fe-*x*Pd-5bredigite and then localized corrosion for Fe-*x*Pd-10bredigite. It can be observed that the Fe-*x*Pd-10bredigite biocomposites corroded most severely with deep corrosion pits on the surface. According to the aforementioned discussion, the excessive bredigite could account for these corrosion pits because the conglomerations observed in Fig. 2 can easily induce the nucleation and growth of localized corrosion. This was likely to induce a self-driven intense pit development and finally a total disintegration of the biocomposites. In general, the 3D topographic results demonstrated similar effects of Pd and bredigite on the corrosion behavior as revealed in the SEM characterization and potentiodynamic tests. The Fe-4Pd-5bredigite biocomposite showed a relatively smooth corrosion morphology with corrosion damage mostly distributed horizontally, indicating a rapid corrosion rate and uniform corrosion

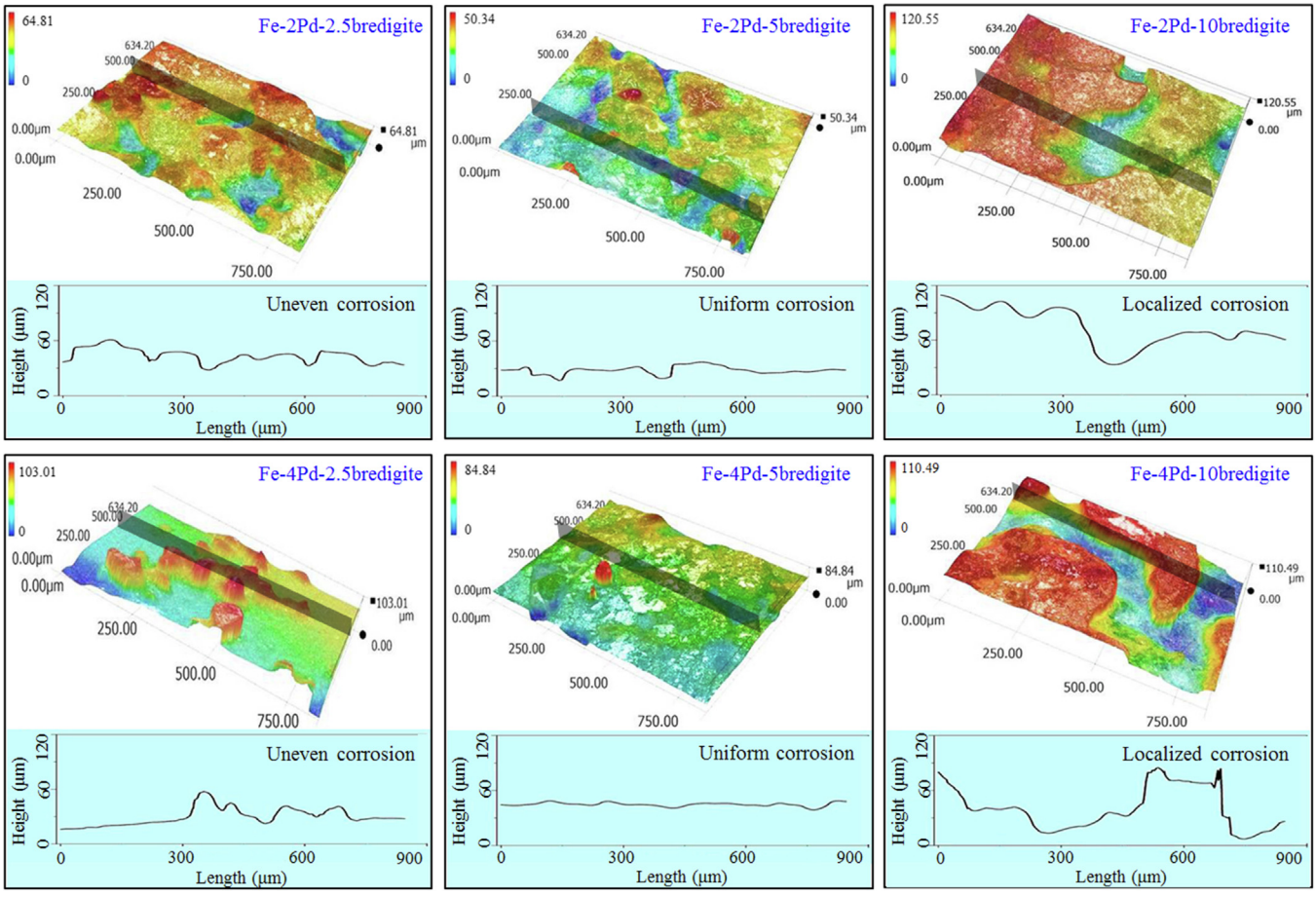

Fig. 6. Three dimensional (3D) surface profile of Fe-Pd-bredigite biocomposites after immersion tests for 21 d and product removal. The height-length graphs represent the height changes along the gray cross-sections.

mode. Therefore, combined with the voluminous apatite precipitation shown in Fig. 5, the Fe-4Pd-5bredigite biocomposite may feature the most attractive biodegradability and bioactivity.

Mechanical properties

The mechanical properties of the biocomposites were investigated by compression tests and microhardness tests and the results are plotted as bar charts in Fig. 7. The compressive yield strength (CYS) of the Fe-2Pd-2.5bredigite biocomposite reached a value of 161 ± 7 MPa and a slight increase was observed with increasing Pd to 4 wt%. Moreover, the addition of Pd also showed a similar effect on the microhardness of the biocomposites. The microhardness of the Fe-4Pd-2.5bredigite biocomposite presented a ~6% increase as compared with that of the Fe-2Pd-2.5bredigite biocomposite. The improvement in mechanical properties could be attributed to the grain refinement, solution strengthening and dispersion strengthening induced by the dissolved Pd within the matrix and the uniformly dispersed Pd-rich IMPs along the grain boundaries. In comparison, bredigite had an opposite influence on the CYS of the biocomposites. The Fe-2Pd-5bredigite biocomposite showed a ~9% drop in CYS as compared with the Fe-2Pd-2.5bredigite biocomposite, followed by a pronounced decrease of ~15% with 10 wt% bredigite addition. A similar trend was also observed in the Fe-4Pd-*x*bredigite biocomposites. The negative influence of bredigite on the CYS might be due to the microstructure inhomogeneity in the biocomposites, such as interfacial mismatch and different deformation mechanisms between metallic and ceramic phases. Moreover, bredigite showed a dual impact on the microhardness. The microhardness of the Fe-*x*Pd-5bredigite biocomposites was 4–6% higher than that of the Fe-*x*Pd-2.5bredigite biocomposites, which could be ascribed to the uniform distribution of the hard bredigite phase within the matrix. However, a significant reduction could be seen in Fe-*x*Pd-10bredigite biocomposites. The mechanical deterioration could be due to brought about by the bredigite conglomerations, causing a weak bonding between the bredigite and matrix. The relatively larger standard deviations also suggested the microstructural inhomogeneity in the Fe-*x*Pd-10bredigite biocomposites.

Cytocompatibility

Cell culture tests were conducted to assess the cytocompatibility of the biocomposites by using MG-63 cells. The biocomposites were separately immersed in DMEM for 3 d and the extracts were then collected and used for cell culture. The cells cultured in DMEM without the extracts served the control. The fluorescence morphology of the cells after 5 d of culture is shown in Fig. 8, in which the live and dead cells are stained in green and red, respectively. It was evident that all the images showed high cell densities with no significant differences among the extracts and the control group, indicating normal proliferation of the cells. Moreover, as can be observed in the higher magnification images, the cells basically maintained a spindle or polygonal morphology with spike-like filopodia, indicating benign responses to the extracts [44]. In addition, the number of live cells slightly decreased as the Pd content increased. This was also revealed by the images of dead cells cultured in the Fe-4Pd-*x*bredigite and the Fe-2Pd-*x*bredigite extracts. In comparison, the live cells presented no visible differences in density among the extracts with different bredigite contents. Furthermore, the cell viabilities of MG-63 cells after 3 and 5 d of culture in the extracts were investigated by CCK-8 tests and the results are expressed as a percentage of that in the control group (Fig. 9). It can be observed that the cell viabilities in the extracts all increased with the prolonged culture period and maintained a value of more than 80%, indicating favorable cytocompatibility of

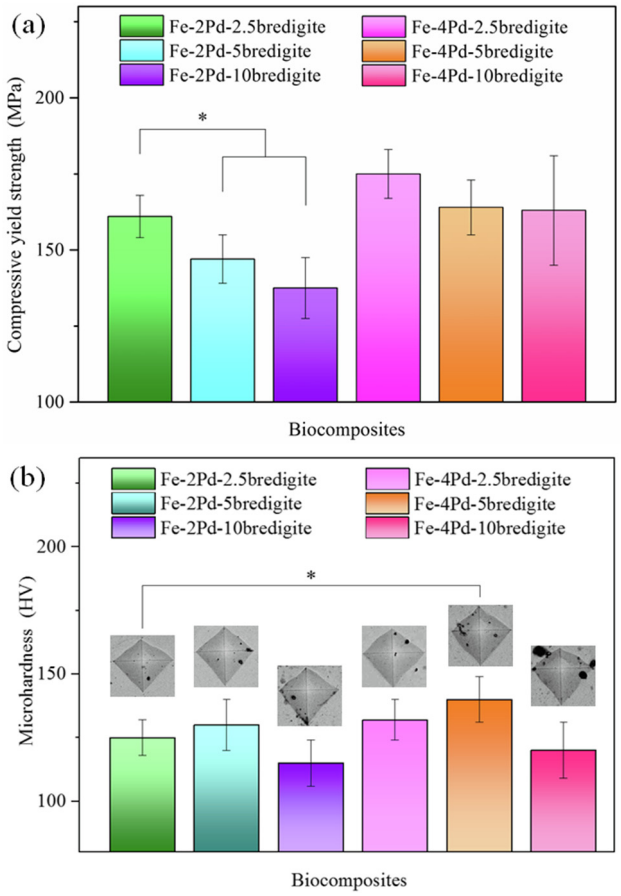

Fig. 7. (a) Compressive yield strength (CYS) and (b) microhardness of Fe-Pd-bredigite biocomposites. The insets represent the SEM morphology of the indentations after microhardness tests ($^{*}P < 0.05$).

the Fe-Pd-bredigite biocomposites to MG-63 cells according to ISO 19003-5. Moreover, the cell viability decreased after being cultured in the Fe-4Pd-2.5bredigite extract compared with the Fe-2Pd-2.5bredigite extract ($P < 0.001$), as well as in the Fe-4Pd-5bredigite extract compared with the Fe-2Pd-5bredigite extract ($P < 0.05$). As for the Fe-4Pd-10bredigite and the Fe-2Pd-10bredigite extracts, cell viability showed no significant difference at 3 d but significant difference at 5 d ($P < 0.001$). It is known that cell proliferation is closely related to the ionic environment of the culture medium [45]. In the present work, on one hand, the degradation rate of the biocomposites was significantly increased with both the contents of Pd and bredigite, which would result in much more release of Fe and Pd ions. This could induce some inhibitory effect on the proliferation of MG-63 cells. On the other hand, the fast release of Ca, Si and Mg ions induced by bredigite degradation might have helped improve the cell proliferation. These results revealed the favorable biocompatibility of the Fe-Pd-bredigite biocomposites to MG-63 cells.

Discussion

An ideal bone implant should have strong bonding with the defective sites, act as a temporary support for cell function, and gradually degrade along with bone tissue regeneration [46,47]. For load-bearing sites, metallic biomaterials are almost the only choice because of the excellent mechanical strengths and processability compared to ceramics and polymers. As a biodegradable metal, Fe has been proposed as potential bone implant biomateri-

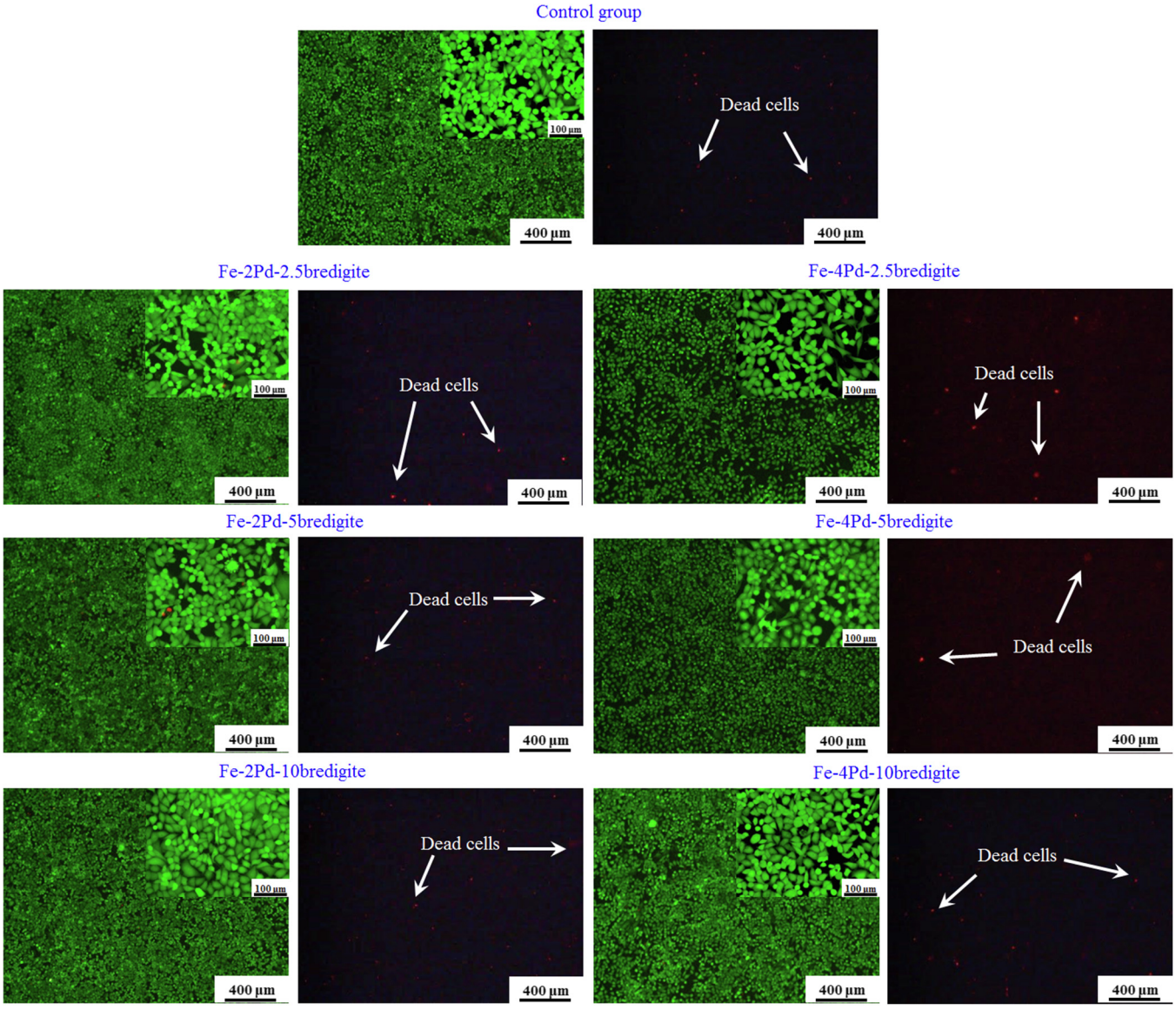

Fig. 8. Fluorescent images of human osteoblast-like cells (MG-63) after 5 d of culture in the extracts, as well as the cells cultured in Dulbecco's modified eagle medium (DMEM) as a control. The live cells are stained green and the dead cells are stained red. (For interpretation of the references to color in this figure legend, the reader is referred to the web version of this article.)

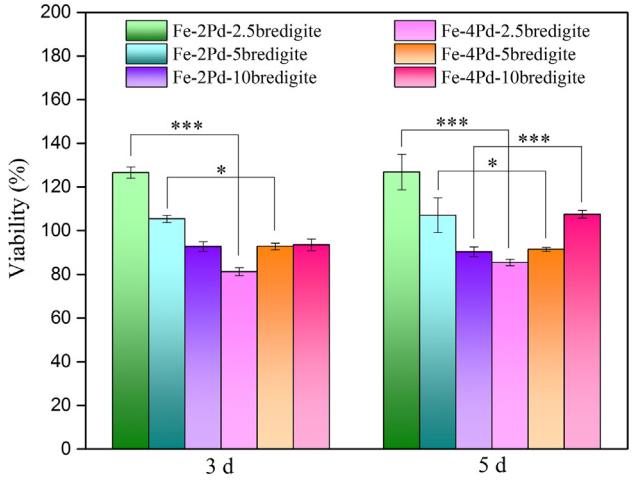

Fig. 9. Cell viabilities of MG-63 cells after 3 and 5 d of culture in the Fe-Pd-bredigite extracts which are expressed as a percentage of that in the control group ($^{*}P < 0.05$; $^{***}P < 0.001$).

als, but the researchers have long been puzzled by the slow degradation and poor bioactivity.

Mechanical properties

In the present work, Pd and bredigite were first combined to improve both the corrosion behavior and bioactivity of Fe for biomedical applications. It is widely accepted that the performance of metal-based composites mainly depends on the microstructure and composition, i.e., the solution elements and precipitates. As revealed by the SEM/EDS images, Pd was partially dissolved in the Fe matrix and the rest formed a nearly continuous network of Pd-rich IMPs along the grain boundaries. In addition, the bredigite phase was also found distributed throughout the biocomposites. The grain size of the Fe matrix gradually decreased with the increase in Pd and bredigite contents. The solid IMPs and bredigite phase were believed to inhibit the grain growth by promoting supercooling and heterogeneous nucleation. In addition, the rapid heating and cooling process of SLM should also be taken into

consideration for the grain refinement. As a result, the refined grain size, together with the dissolved Pd and dispersed Pd-rich IMPs, contributed to the improvement of CYS by immobilizing dislocations and thus inducing more deformation resistance. In comparison, bredigite showed a negative influence on CYS, which be due to the microstructure inhomogeneity, such as interfacial mismatch and different deformation mechanisms between metals and ceramics [48]. Nevertheless, the microhardness of the biocomposites was improved after the addition of bredigite, which could be ascribed to the uniform distribution of the hard bredigite phase within the matrix. Consequently, the CYS and microhardness of the Fe-Pd-bredigite biocomposites were tailored to 164 MPa and 140 HV, respectively, which were comparable to those of the native bone [49,50].

Degradation behavior

Fig. 10 illustrates the corrosion process of the prepared Fe-Pd-bredigite biocomposites in the SBF solution. It is known that grain boundaries are relatively distorted areas with a configuration of dislocations and lattice mismatch [51,52]. When immersed in the SBF solution, corrosion first started from the Fe matrix closely around the Pd-rich IMPs at the grain boundaries. The Pd-rich IMPs with high corrosion potential as cathodes formed micro-galvanic cells with the Fe matrix as anodes. The Fe matrix was then oxidized into ferrous ions, and the electrons generated from the dissolving Fe were transferred to the Pd-rich IMPs where the electrons were consumed by oxygen reduction (Fig. 10a). This resulted in solution alkalization near the IMPs, followed by the formation of ferrous hydroxide and ferric hydroxide at the early stage of immersion. As aforementioned, the IMPs consisted of high amounts of Pd with a high standard reduction potential. Therefore, the resulting Pd-rich IMPs were expected to be much nobler than the Fe matrix. The large potential difference promoted the electron transfer and thus the reaction rate of anodes. Moreover, the Pd-rich IMPs existed as a nearly continuous network along the grain boundaries, indicating the large amount of micro-galvanic cells in the biocomposites. Thus, the presence of the Pd-rich IMPs induced tremendous micro-galvanic corrosion significantly increasing the corrosion rate of the Fe matrix.

In addition, the physical presence of the bredigite phase generated more sites that were vulnerable to corrosion attack due to the excellent biodegradability [53]. As a promising bioactive ceramics, bredigite can rapidly hydrolyze in a biological environment. It has been reported that the biodegradation rate of bredigite was faster than those of HAP [54], diopside and akermanite bioceramics [55], and was comparable to that of β-tricalcium phosphate bioceramics [56], which was known for the very fast degradation for bone repair [57]. Thus, the bredigite phase would rapidly corrode and dissolve from the Fe matrix, leaving corrosion pits in situ (Fig. 10b). These corrosion pits exposed more Fe matrix to the corrosion medium, thereby accelerating the corrosion process. Furthermore, bredigite and Fe belong to ceramics and metals, respectively, with different physiochemical properties. Some defects or even conglomerations at the Fe-bredigite interfaces after the SLM process could result. The interfacial defects acted as channels for further invasion of the corrosion medium into the Fe matrix. These were confirmed by the electrochemical and immersion results, in which the corrosion rate increased with bredigite content. Similar influences of ceramic phase on the interfacial characteristics and corrosion behavior of metallic matrix were also reported in many other MMCs, such as Zn-HAP composites [43]

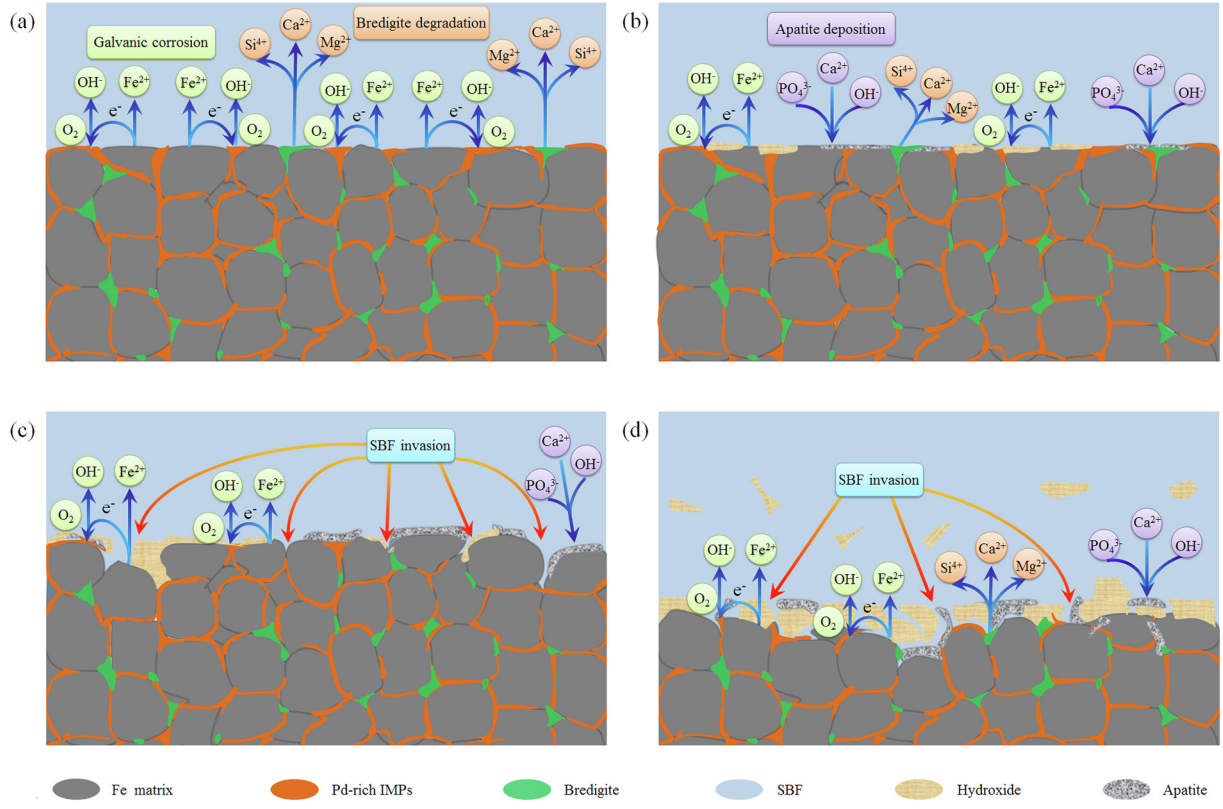

Fig. 10. Schematic of the degradation process of Fe-Pd-bredigite biocomposites: (a) galvanic corrosion between Pd-rich intermetallic phases (IMPs) and the Fe matrix, as well as bredigite degradation; (b) hydroxide formation and apatite deposition on the surface; (c) simulated body fluid (SBF) invasion via the corrosion pits resulting from bredigite degradation; (d) exposure of fresh Fe matrix to the SBF, followed by a continuous degradation.

and Fe-HAP composites [58]. Moreover, bredigite contributed to the spontaneous absorption and induction of Ca^{2+} and PO_4^{3-} deposition from the SBF solution, thus leading to the rapid apatite formation on the Fe surface. Previous studies have also reported that bredigite possessed higher bioactivity than HAP and could stimulate apatite nucleation and growth, which is beneficial for the rapid synostosis with the native bone [59]. With time, the corrosion area rapidly expanded into the fresh Fe matrix beneath the IMPs and bredigite (Fig. 10c). Then, the exposed Fe matrix was further corroded and replaced by voluminous degradation products and apatite layer. Therefore, the newly developed Fe-Pd-bredigite biocomposites, especially the Fe-4Pd-5bredigite, featured a significantly accelerated degradation and excellent bioactivity.

Cytocompatibility

Biocompatibility is still the biggest hindrance of biodegradable metallic implants for biomedical applications. This issue is mainly caused by the released metallic ions and degradation products which can affect cell metabolic activities and proliferation. In the present work, it can be observed that the biocomposites showed increased cytotoxicity after the addition of Pd. On one hand, the cytotoxicity should be mainly attributed to the released Fe^{2+} and Fe^{3+} ions. It has been reported that excess Fe^{2+} and Fe^{3+} ions would catalyze the formation of radicals, thereby damaging the cell structure [60]. The galvanic cells formed between Pd-rich IMPs and the Fe matrix significantly accelerated the degradation of the biocomposites, resulting in a rapid release of large amounts of Fe^{2+} and Fe^{3+} ions. On the other hand, Pd ions are capable of eliciting *in vitro* a number of cytotoxic effects by stimulating free radical production and the degree of cytotoxicity corresponds to the solubility of Pd compounds [61,62]. In this study, the concentration of Pd ions released was very low because Pd had a very limited dissolution in the human body and showed nontoxicity in elemental form. Moreover, the released Pd ions can also be rapidly excreted from the body via the feces and urine. Recent studies also reported acceptable cytocompatibility of Pd at 2 wt% and 5 wt% [63]. Moreover, bredigite is one of the frequently used bioactive ceramics for bone repair owing to the excellent biocompatibility and bioactivity. The release of Ca^{2+}, Si^{4+} and Mg^{2+} from bredigite could stimulate cell proliferation and differentiation and then promote new bone formation. Furthermore, the Ca-Mg-P precipitates induced by bredigite have been proven to facilitate the adsorption of cell-related proteins, such as fibronectin and vitronectin [54]. Therefore, although the adverse effects of Pd exerted on cell proliferation were observed, the morphology and proliferation of MG-63 cells cultured in the extracts were comparable with those in the control group, which indicated high biocompatibility of the biocomposites without noticeable cytotoxicity.

Conclusions

The present work aimed to develop an Fe-Pd-bredigite biocomposite with a well-balanced combination of accelerated degradation, excellent bioactivity, suitable mechanical properties and favorable cytocompatibility for biomedical applications.

(1) Most Pd formed noble IMPs as a nearly continuous network along the grain boundaries. The grain size of the biocomposites was refined after the addition of Pd and bredigite.
(2) The degradation rates of the biocomposites were significantly increased due to the tremendous micro-galvanic corrosion between noble Pd-rich IMPs and the Fe matrix. Moreover, the preferential degradation of bredigite also accounted for the accelerated degradation by providing more channels for corrosion medium penetration.
(3) The Fe-4Pd-5bredigite biocomposite presented a good combination of rapid and uniform degradation with voluminous degradation products. Moreover, the presence of bredigite facilitated the rapid apatite formation on the Fe surface, indicating the excellent bioactivity of the biocomposites.
(4) The Pd-rich IMPs and dissolved Pd were deployed in the biocomposites with improved CYS and hardness. However, a bredigite content of 10 wt% caused deteriorated mechanical properties and localized corrosion.
(5) Although the presence of Pd and accelerated release of Fe ions had an inhibitory effect on MG-63 cells, the biocomposites still showed favorable biocompatibility with no significant difference in cell proliferation as compared with the control group.
(6) The Fe-4Pd-5bredigite biocomposite achieved an optimum combination of suitable biodegradation, bioactivity, biocompatibility, and mechanical properties.

Conflict of interest

The author have declared no conflict of interest.

Compliance with Ethics Requirements

This article does not contain any studies with human or animal subjects.

Acknowledgements

This work was supported by the following funds: (1) The Natural Science Foundation of China (51705540, 81871494, 81871498); (2) Hunan Provincial Natural Science Foundation of China (2018JJ3671, 2019JJ50588); (3) Guangdong Province Higher Vocational Colleges & Schools Pearl River Scholar Funded Scheme (2018); (4) The Open Sharing Fund for the Large-scale Instruments and Equipments of Central South University; (5) The Project of Hunan Provincial Science and Technology Plan (2017RS3008); (6) Shenzhen Science and Technology Plan Project (JCYJ20170817112445033); (7) National Postdoctoral Program for Innovative Talents (BX201700291); (8) The China Postdoctoral Science Foundation (2018M632983).

References

[1] Shuai C, Wang B, Yang Y, Peng S, Gao C. 3D honeycomb nanostructure-encapsulated magnesium alloys with superior corrosion resistance and mechanical properties. Compos Part B – Eng 2019;162:611–20.
[2] Silva B, Faustino P. An overview of molecular basis of iron metabolism regulation and the associated pathologies. Biochim Biophys Acta Mol Basis Dis 2015;1852(7):1347–59.
[3] Cheng J, Huang T, Zheng YF. Microstructure, mechanical property, biodegradation behavior, and biocompatibility of biodegradable Fe-Fe2O3 composites. J Biomed Mater Res A 2014;102(7):2277–87.
[4] Allenstein U, Ma Y, Arabi-Hashemi A, Zink M, Mayr SG. Fe–Pd based ferromagnetic shape memory actuators for medical applications: biocompatibility, effect of surface roughness and protein coatings. Acta Biomater 2013;9(3):5845–53.
[5] Sikora E. A quest for the holy grail of bioimplants – a review of recent developments in biodegradable metals for medical applications. Recent Pat Corros Sci 2012;2(2):81–97.
[6] Gao C, Peng S, Feng P, Shuai C. Bone biomaterials and interactions with stem cells. Bone Res 2017;5:17059.
[7] Feng P, Wu P, Gao C, Yang Y, Guo W, Yang W, et al. A multimaterial scaffold with tunable properties: toward bone tissue repair. Adv Sci 2018;1700817.
[8] Feng P, He J, Peng S, Gao C, Zhao Z, Xiong S, et al. Characterizations and interfacial reinforcement mechanisms of multicomponent biopolymer based scaffold. Mater Sci Eng C – Mater Biol Appl 2019;100:809–25.
[9] Shuai C, Li S, Peng S, Feng P, Lai Y-X, Gao C. Biodegradable metallic bone implants. Mater Chem Front 2019;3:544–62.
[10] Shuai C, Xu Y, Feng P, Wang G, Xiong S, Peng S. Antibacterial polymer scaffold based on mesoporous bioactive glass loaded with in situ grown silver. Chem Eng J 2019.

[11] Cheng J, Huang T, Zheng Y. Relatively uniform and accelerated degradation of pure iron coated with micro-patterned Au disc arrays. Mater Sci Eng C – Mater Biol Appl 2015;48:679–87.
[12] Huang T, Zheng Y. Uniform and accelerated degradation of pure iron patterned by Pt disc arrays. Sci Rep 2016;6:23627.
[13] Li J, Cao P, Zhang X, Zhang S, He Y. *In vitro* degradation and cell attachment of a PLGA coated biodegradable Mg–6Zn based alloy. J Mater Sci 2010;45 (22):6038–45.
[14] Zhou J, Yang Y, Alonso Frank M, Detsch R, Boccaccini AR, Virtanen S. Accelerated degradation behavior and cytocompatibility of pure iron treated with sandblasting. ACS Appl Mater Inter 2016;8(40):26482–92.
[15] Bagherifard S, Hickey DJ, Fintová S, Pastorek F, Fernandez-Pariente I, Bandini M, et al. Effects of nanofeatures induced by severe shot peening (SSP) on mechanical, corrosion and cytocompatibility properties of magnesium alloy AZ31. Acta Biomater 2018;66:93–108.
[16] Jurgeleit T, Quandt E. Zamponi C. Magnetron sputtering a new fabrication method of iron based biodegradable implant materials. Adv Mater Sci Eng 2015.
[17] Moravej M, Prima F, Fiset M, Mantovani D. Electroformed iron as new biomaterial for degradable stents: Development process and structure–properties relationship. Acta Biomater 2010;6(5):1726–35.
[18] Obayi CS, Tolouei R, Paternoster C, Turgeon S, Okorie BA, Obikwelu DO, et al. Influence of cross-rolling on the micro-texture and biodegradation of pure iron as biodegradable material for medical implants. Acta Biomater 2015;17:68–77.
[19] Schinhammer M, Hänzi AC, Löffler JF, Uggowitzer PJ. Design strategy for biodegradable Fe-based alloys for medical applications. Acta Biomater 2010;6 (5):1705–13.
[20] Čapek J, Kubásek J, Vojtěch D, Jablonská E, Lipov J, Ruml T. Microstructural, mechanical, corrosion and cytotoxicity characterization of the hot forged FeMn30(wt.%) alloy. Mater Sci Eng C – Mater Biol Appl 2016;58:900–8.
[21] Drevet R, Zhukova Y, Malikova P, Dubinskiy S, Korotitskiy A, Pustov Y, et al. Martensitic transformations and mechanical and corrosion properties of Fe-Mn-Si alloys for biodegradable medical implants. Metall Mater Trans A 2018;49(3):1006–13.
[22] Liu B, Zheng YF. Effects of alloying elements (Mn Co, Al, W, Sn, B, C and S) on biodegradability and *in vitro* biocompatibility of pure iron. Acta Biomater 2011;7(3):1407–20.
[23] Hufenbach J, Wendrock H, Kochta F, Kühn U, Gebert A. Novel biodegradable Fe-Mn-C-S alloy with superior mechanical and corrosion properties. Mater Lett 2017;186:330–3.
[24] Chen YZ, Xu Q, Yu SH, Jiang HL. Tiny Pd@ Co core–shell nanoparticles confined inside a metal–organic framework for highly efficient catalysis. Small 2015;11 (1):71–6.
[25] Fanelli M, Formica M, Fusi V, Giorgi L, Micheloni M, Paoli P. New trends in platinum and palladium complexes as antineoplastic agents. Coord Chem Rev 2016;310:41–79.
[26] Matusiewicz H. Potential release of *in vivo* trace metals from metallic medical implants in the human body: from ions to nanoparticles–a systematic analytical review. Acta Biomater 2014;10(6):2379–403.
[27] Huang T, Cheng J, Zheng YF. *In vitro* degradation and biocompatibility of Fe–Pd and Fe–Pt composites fabricated by spark plasma sintering. Mater Sci Eng C – Mater Biol Appl 2014;35(2):43–53.
[28] Jarzabek DM, Chmielewski M, Dulnik J, Strojny-Nedza A. The influence of the particle size on the adhesion between ceramic particles and metal matrix in MMC composites. J Mater Eng Perform 2016;25(8):3139–45.
[29] Eilbagi M, Emadi R, Raeissi K, Kharaziha M, Valiani A. Mechanical and cytotoxicity evaluation of nanostructured hydroxyapatite-bredigite scaffolds for bone regeneration. Mater Sci Eng C – Mater Biol Appl 2016;68:603–12.
[30] Kouhi M, Shamanian M, Fathi M, Samadikuchaksaraei A, Mehdipour A. Synthesis, characterization, *in vitro* bioactivity and biocompatibility evaluation of hydroxyapatite/bredigite (Ca 7 MgSi 4 O 16) composite nanoparticles. JOM 2016;68(4):1–10.
[31] Sikora-Jasinska M, Paternoster C, Mostaed E, Tolouei R, Casati R, Vedani M, et al. Synthesis, mechanical properties and corrosion behavior of powder metallurgy processed Fe/Mg2Si composites for biodegradable implant applications. Mater Sci Eng C – Mater Biol Appl 2017;81:511–21.
[32] Montufar E, Casas-Luna M, Horynová M, Tkachenko S, Fohlerová Z, Diaz-de-la-Torre S, et al. High strength, biodegradable and cytocompatible alpha tricalcium phosphate-iron composites for temporal reduction of bone fractures. Acta Biomater 2018;70:293–303.
[33] Wang M, Song B, Wei Q, Zhang Y, Shi Y. Effects of annealing on the microstructure and mechanical properties of selective laser melted AlSi7Mg alloy. Mat Sci Eng A – Struct 2019;739:463–72.
[34] Shuai C, Guo W, Wu P, Yang W, Hu S, Xia Y, et al. A graphene oxide-Ag co-dispersing nanosystem: dual synergistic effects on antibacterial activities and mechanical properties of polymer scaffolds. Chem Eng J 2018;347:322–33.
[35] Shuai C, Zan J, Qi F, Wang G, Liu Z, Yang Y, et al. nMgO-incorporated PLLA bone scaffolds: Enhanced crystallinity and neutralized acidic products. Mater Des 2019;174:107801.
[36] Cai C, Radoslaw C, Zhang J, Yan Q, Wen S, Song B, et al. In-situ preparation and formation of TiB/Ti-6Al-4V nanocomposite via laser additive manufacturing: Microstructure evolution and tribological behavior. Powder Technol 2019;342:73–84.
[37] Shuai C, Cheng Y, Yang Y, Peng S, Yang W, Qi F. Laser additive manufacturing of Zn-2Al part for bone repair: Formability, microstructure and properties. J Alloys Compd 2019.
[38] Zhang J, Song B, Wei Q, Bourell D, Shi Y. A review of selective laser melting of aluminum alloys: Processing, microstructure, property and developing trends. J Mater Sci Technol 2019;35(2):270–84.
[39] Polívková M, Siegel J, Rimpelová S, Hubáček T, Kolská Z, Švorčík V. Cytotoxicity of Pd nanostructures supported on PEN: Influence of sterilization on Pd/PEN interface. Mater Sci Eng C – Mater Biol Appl 2017;70(Pt 1):479–86.
[40] Sangeetha K, Girija EK. Effect of alginate on hydroxyapatite/gelatin nanocomposites for orthopedic applications. J Bionanosci 2016;10(4):257–66.
[41] Bagherifard S, Beretta N, Monti S, Riccio M, Bandini M, Guagliano M. On the fatigue strength enhancement of additive manufactured AlSi10Mg parts by mechanical and thermal post-processing. Mater Des 2018;145:28–41.
[42] Baicheng Z, Xiaohua L, Jiaming B, Junfeng G, Pan W, Chen-nan S, et al. Study of selective laser melting (SLM) Inconel 718 part surface improvement by electrochemical polishing. Mater Des 2017;116:531–7.
[43] Yang H, Qu X, Lin W, Wang C, Zhu D, Dai K, et al. *In vitro* and *in vivo* studies on zinc-hydroxyapatite composites as novel biodegradable metal matrix composite for orthopedic applications. Acta Biomater 2018;71:200–14.
[44] Shuai C, Feng P, Wu P, Liu Y, Liu X, Lai D, et al. A combined nanostructure constructed by graphene and boron nitride nanotubes reinforces ceramic scaffolds. Chem Eng J 2017;313:487–97.
[45] Cunha CBD, Klumpers DD, Koshy ST, Weaver JC, Chaudhuri O, Seruca R, et al. CD44 alternative splicing in gastric cancer cells is regulated by culture dimensionality and matrix stiffness. Biomaterials 2016;98:152–62.
[46] Gupta P, Adhikary M, Jc M, Kumar M, Bhardwaj N, Mandal BB. Biomimetic, osteoconductive non-mulberry silk fiber reinforced tricomposite scaffolds for bone tissue engineering. ACS Appl Mater Inter 2016;8(45):30797–810.
[47] Shuai C, Li Y, Wang G, Yang W, Peng S, Feng P. Surface modification of nanodiamond: toward the dispersion of reinforced phase in poly-l-lactic acid scaffolds. Int J Biol Macromol 2019;126:1116–24.
[48] Dezfuli SN, Huan Z, Leeflang S, Jiang C, Zhou J. Fabrication of novel magnesium-matrix composites and their mechanical properties prior to and during *in vitro* degradation. J Mech Behav Biomed 2016;67:74–86.
[49] Evans FG, Bang S. Differences and relationships between the physical properties and the microscopic structure of human femoral, tibial and fibular cortical bone. Am J Anat 1967;120(1):79–88.
[50] Ogueri KS, Jafari T, Ivirico JLE, Laurencin CT. Polymeric Biomaterials for Scaffold-Based Bone Regenerative Engineering. Regen Eng Transl Med 2018:1–27.
[51] Deng J, Dong K, Yang P, Peng Y, Ju G, Hu J, et al. Large lattice mismatch effects on the epitaxial growth and magnetic properties of FePt films. J Magn Magn Mater 2018;446:125–34.
[52] Wang L, Sun N, Wang Z, Han H, Yang Y, Liu R, et al. Self-assembly of mixed dodecylamine–dodecanol molecules at the air/water interface based on large-scale molecular dynamics. J Mol Liq 2019;276:867–74.
[53] Zhou Y, Wu C, Zhang X, Han P, Xiao Y. The ionic products from bredigite bioceramics induced cementogenic differentiation of periodontal ligament cells via activation of the Wnt/β-catenin signalling pathway. J Mater Chem B 2013;1(27):3380–9.
[54] Dezfuli SN, Huan Z, Mol A, Leeflang S, Chang J, Zhou J. Advanced bredigite-containing magnesium-matrix composites for biodegradable bone implant applications. Mater Sci Eng C-Mater Biol Appl 2017;79:647–60.
[55] Wu C, Chang J. Degradation, bioactivity, and cytocompatibility of diopside, akermanite, and bredigite ceramics. J Biomed Mater Res B Appl Biomater 2007;83(1):153–60.
[56] Wu C, Chang J, Zhai W, Ni S. A novel bioactive porous bredigite (Ca7MgSi4O16) scaffold with biomimetic apatite layer for bone tissue engineering. J Mater Sci Mater Med 2007;18(5):857–64.
[57] Karadjian M, Essers C, Tsitlakidis S, Reible B, Moghaddam A, Boccaccini AR, et al. Biological Properties of Calcium Phosphate Bioactive Glass Composite Bone Substitutes: Current Experimental Evidence. Int J Mol Sci 2019;20(2):305.
[58] Dehestani M, Adolfsson E, Stanciu LA. Mechanical properties and corrosion behavior of powder metallurgy iron-hydroxyapatite composites for biodegradable implant applications. Mater Des 2016;109:556–69.
[59] Gao C, Feng P, Peng S, Shuai C. Carbon nanotube, graphene and boron nitride nanotube reinforced bioactive ceramics for bone repair. Acta Biomater 2017;61:1–20.
[60] Henle ES, Luo Y, Linn S. Fe2+, Fe3+, and oxygen react with DNA-derived radicals formed during iron-mediated Fenton reactions. Biochemistry 1996;35 (37):12212–9.
[61] Leso V, Iavicoli I. Palladium nanoparticles: toxicological effects and potential implications for occupational risk assessment. Int J Mol Sci 2018;19(2):503.
[62] Iavicoli I, Bocca B, Fontana L, Caimi S, Bergamaschi A, Alimonti A. Distribution and elimination of palladium in rats after 90-day oral administration. Toxicol Ind Health 2010;26(3):183–9.
[63] Čapek J, Msallamová Š, Jablonská E, Lipov J, Vojtěch D. A novel high-strength and highly corrosive biodegradable Fe-Pd alloy: Structural, mechanical and *in vitro* corrosion and cytotoxicity study. Mater Sci Eng C – Mater Biol Appl 2017;79:550–62.